Volume 19
Number 6
14 February 2023
Pages 1049–1260

Soft Matter

rsc.li/soft-matter-journal

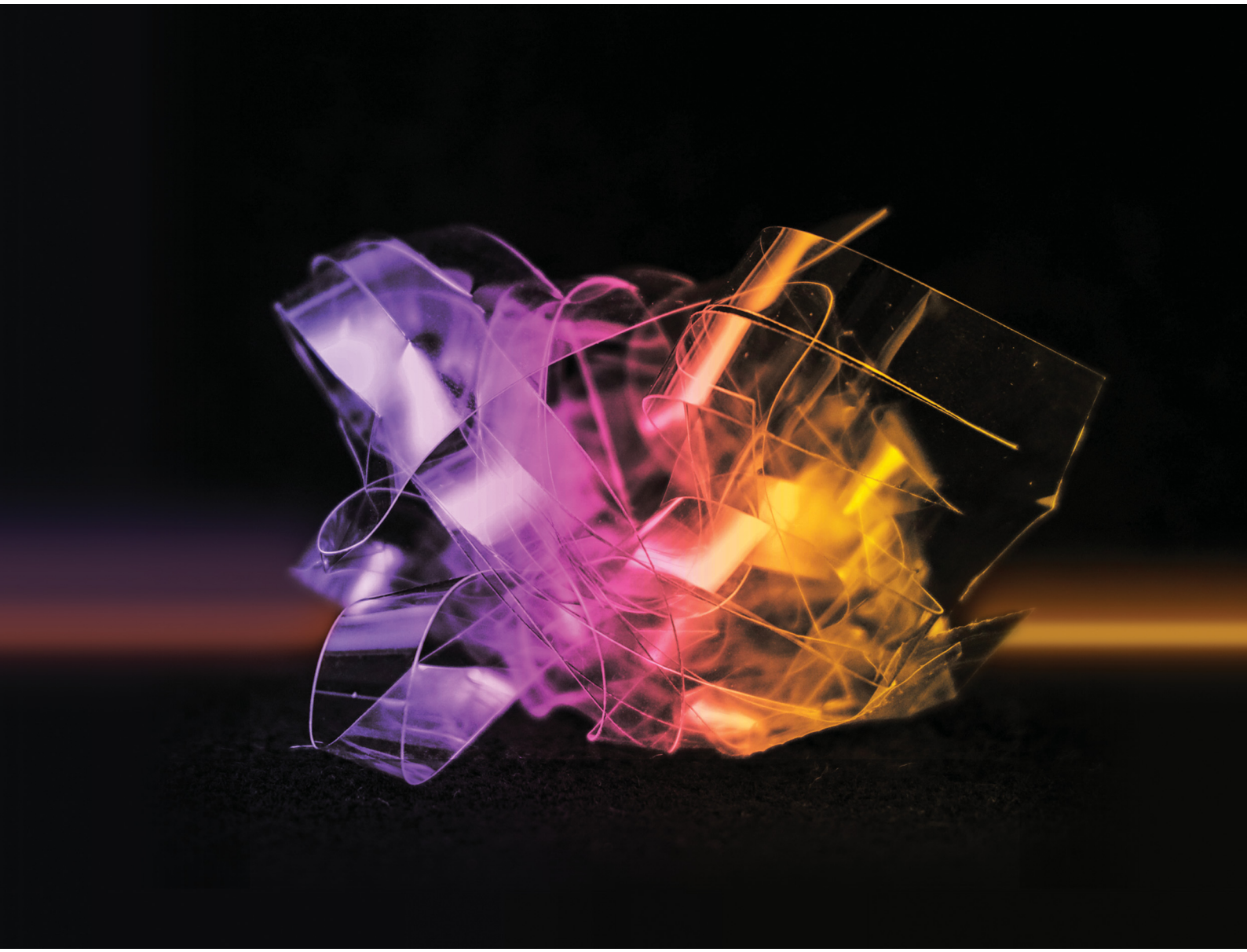

ISSN 1744-6848

ROYAL SOCIETY OF CHEMISTRY

PAPER
Andrew B. Croll *et al.*
Crumpled Kirigami

Soft Matter

PAPER

View Article Online
View Journal | View Issue

Check for updates

Cite this: *Soft Matter*, 2023, **19**, 1081

Crumpled Kirigami†

Wathsala M. A. Jayawardana, ‡[a] Yangchao Liao, ‡[b] Zhaofan Li, [b] Wenjie Xia [bc] and Andrew B. Croll *[ac]

Received 2nd December 2022,
Accepted 18th January 2023

DOI: 10.1039/d2sm01584f

rsc.li/soft-matter-journal

When a thin sheet is confined to a volume much smaller than its length (or width), it forms a complex state of sharp bends, point-like developable cones (d-cones) and extended ridges known as crumpled matter. One interesting feature of this state, is its high resistance to compression given its light weight. While the origins of this strength still remain a matter of debate, much has been learned through simple experiments and models. Very little work has explored how crumpling is affected by the sheet's topology, which is curious given the close relation between geometry and mechanics. In this work, we couple confocal microscopy with simple force experiments and coarse-grained molecular dynamics (CG-MD) simulations to explore how adding cuts to a sheet alters its behavior in the crumpled state. We find that cutting does not significantly alter the overall compressive behaviour: force scales as a power law irrespective of cuts and magnitudes are only slightly reduced by cutting. Remarkably, when examining regions of high curvature in the crumpled sheets we see evidence of significant changes in the distribution of curvature in cut sheets.

Open Access Article. Published on 19 January 2023. Downloaded on 7/17/2025 10:22:53 PM.
This article is licensed under a Creative Commons Attribution-NonCommercial 3.0 Unported Licence.

1 Introduction

When a nearly two-dimensional (2D) sheet of paper is crushed into a tight ball, it is said to be crumpled. Crumpled materials can be found many places in our day-to-day life serving biological or engineered purposes. Examples include viral capsids,[1,2] delicate pieces of flower petals packed inside a flower bud,[3] brain cortex[4] and even on large scales such as Geological formations.[5] Paper crumples are commonly used as protective layers for fragile objects, in part because paper typically comes in sheets and can be more environment friendly than specially engineered polymer foams[6] or bubble wraps[7] which are typically made of non-biodegradable materials. In general, crumpled matter is useful because it has properties such as a high strength to density ratio (the volume of a hand crushed paper crumple can be more than 75% air[8]), high deformability, high energy absorption, and ultimately crumples are very easily fabricated. Scientists and engineers have studied crumpled matter in earnest because of the complexity of these structures and because of their curiosity as to how the useful macroscopic properties arise.

Understanding the cause of the crumples rigidity has often focused on identifying the basic structural features that occur in a crumpled ball (Fig. 1). Studies have thus far identified four

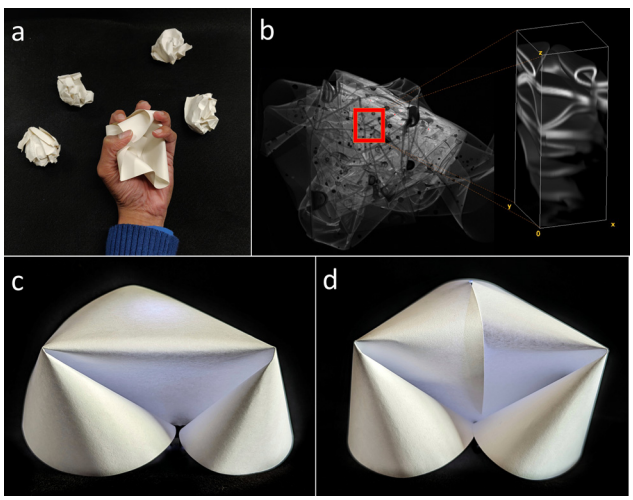

Fig. 1 Schematic overview of experimental concept. (a) The hand crumple. (b) 2D and 3D Confocal images of a PDMS crumple. (c) Top view of a ridge (ridge a bend in-between two d-cones that requires in-plane stretching). (d) Top view of a ridge when there is a cut in the middle which releases the stretching stored in the ridge creating two isolated d-cones. (Photographs of c and d taken with extra back light to see the structure properly).

[a] *Department of Physics, North Dakota State University, Fargo, USA. E-mail: Andrew.Croll@ndsu.edu*
[b] *Department of Civil, Construction and Environmental Engineering, North Dakota State University, Fargo, ND, USA*
[c] *Materials and Nanotechnology, North Dakota State University, Fargo, USA*

† Electronic supplementary information (ESI) available: Additional simulation details and discussion of high curvature structural statistics. See DOI: https://doi.org/10.1039/d2sm01584f

‡ These authors contributed equally to this work.

Open Access Article. Published on 19 January 2023. Downloaded on 7/17/2025 10:22:53 PM.
This article is licensed under a Creative Commons Attribution-NonCommercial 3.0 Unported Licence.

structural ''building blocks'' – bends, folds, ridges, and point-like peaks developable cones (d-cones) that might be important in the overall structure.[8–10] A bend is weakly defined as a region of sheet where the radius of curvature is smaller than other adjacent regions of sheet. A sharper bend, typically where plastic damage has occurred is termed a fold. If present, the plasticity will lead to memory formation in the sheet, which is often a focus of analytic models of crumpling.[11–13] A point-like peak is called a developable cone or d-cone (Fig. 1c and d). More accurately, a d-cone is a conical dislocation in the structure due to focused, localized stretching at the peak of the cone only (the sheet is unstretched elsewhere in the cone). A ridge is a smooth structure which requires in-plane stretching and joins two d-cones (Fig. 1c). Research has still not definitively identified which structural feature dominates the rigidity of the crumple.

In this work, we focus on modifying the sheet topology in order to limit long-range structure formation. The work is motivated by two observations. First, if a ridge forms during confinement, large energies are required due to the in-plane stretching.[8] However, if the sheet between the two d-cones is cut, stretching is no longer necessary or possible (Fig. 1c and d). Secondly, the observation that few d-cones form near the edges of unaltered crumpled sheets suggests that energy is reduced during compression if d-cones are able to form 'virtually' (that is such that their cores are off the sheet).[14] Therefore, we aim to directly test how vastly increased sheet edge boundaries influence the compressive strength of crumpled matter.

Origami ('ori', fold; 'kami', paper), the paper-folding art form in which a flat sheet of paper is folded into a desired structure, has inspired the design of many useful light-weight structures.[15–18] Such ordered structures differ from random crumples in many ways but are also created from the same four basic building blocks described above. Typically, origami structures are dominated by folds and d-cones, though occasionally they include less focused bending. Researchers have also noted that adding cuts to a sheet, Kirigami ('kiri', cut; 'kami', paper), facilitates a much wider design space. Kirigami can be designed to allow parts of a sheet to rotate, either within the plane of the sheet, or out of the plane of the sheet, creating auxetic or other uncommon global deformation modes.[19] In short, cuts allow new mechanisms of motion and energy storage that typically don't occur in an uncut cut sheet. There has been little exploration of how confinement would affect the unusual deformation mechanisms available in kirigami systems.

Previous crumpling studies have attempted to identify how folds, ridges, and bends affect the rigidity of a crumple. Matan and coworkers created a scaling model based on the assumed dominance of ridges.[8] The model predicted that forces would rise as $F(H) \sim F_0 H^{-\alpha}$, where H is the degree of compression, F_0 is the power-law amplitude, and α is a power-law exponent predicted to be a universal value of 8/3. Early simulations showed some agreement. Vliegenthart and Gompper, for example, found a near 8/3 exponent in simulations of a phantom sheet, but found a larger exponent of approximately 4 for more realistic self-avoiding sheets.[20,21]

Deboeuf and coworkers developed another theory based on the number of folds in a crumple.[9] The model begins with the notion that sheet folding requires a force proportional to modulus and sheet thickness squared. Additionally, they also show how a power law might emerge for a crumpled sheet but note that the exponent would depend on how the sheet is successively folded. They predicted a range of power law exponents is possible (1 to 4).

We have developed a similar model, but assume a more empirical starting point. By exploring the details of the amplitude of the power law, in addition to its exponent, we arrived at the conclusion that bending is the key generator of force (as in Deboeuf), but that long range assemblies of curvature (folds) are not important. Our conceptual point of view is that d-cones (specifically their cores) form the key high energy structure. Extended folds, from this point of view, are simply loci of d-cone cores. Thus, the total length of folds is simply a proxy for how many d-cones were formed during the time the sheet is being confined. A fold's direction or path (or fragmention) is not important to the overall energy.[10] As we don't yet have proof of these features, we consider this model empirical. From this point of view a scaling argument can be made. The force to bend a region of sheet to a curvature of order $1/t$, where t is the sheet thickness, scales as $F \sim Et^2$. The compressing plates only matter when $H < 2R$ where R is the radius of the crumpled sheet so confinement can only add *via* a unitless factor of $2R/H$. The total structure must then support a load given by,

$$F = Et^2\left(\frac{2Ro}{H}\right)^{\alpha}, \quad (1)$$

where E is the Young's modulus and we assume the power α is related to material properties and the network of high curvature features in the sheet. However, there remains no direct evidence that any one substructure is dominant in crumpling so it is important to narrow down possible causes in order to develop a deeper fundamental understanding of important emergent properties of crumpled matter.

Material properties are also known to affect the rigidity of a crumple.[22] A fold made in plastic material will create memory as curvatures reach high values and plastically deform the sheets. In fact, many schemes exist to analyse these sharp fold patterns after a crumpled sheet is opened.[11–13] On the other hand, low adhesion elastic sheets retain no memory of high curvatures but still show similar compression behaviour when crumpled. Ensembles of measurements show not only different values for the average exponents but different distributions of exponents for the different materials, which differ again when surface adhesion is changed.[10,22,23] It is therefore important to take those material properties into account when examining the effect of structural features inside a crumple.

Remarkably, there have been few attempts to explore how the topology of the sheet affects the crumpling process. In an attempt to create a porous crumpled material, Mirizelli and coworkers explored the mechanical behavior of crumpled sheets with hole patterns cut in them.[24] They found a tiny increase in the exponent of a power-law describing the force as

 This journal is © The Royal Society of Chemistry 2023

Open Access Article. Published on 19 January 2023. Downloaded on 7/17/2025 10:22:53 PM.
This article is licensed under a Creative Commons Attribution-NonCommercial 3.0 Unported Licence.

a function of displacement as the crumple was crushed by a mesh approximating a three-dimensional (3D) compression, and some evidence for alignment of folds with the holes.

Additionally, the previous studies explored the crumpling behavior of damaged and defective sheets through molecular dynamics (MD) simulations. It was found that the conformation of graphene sheets at equilibrium was significantly affected by the introduced random vacancies, *i.e.*, the increase in vacancy ratio caused the sheet to transition from a flat conformation to a crumpled morphology and a more amorphous carbon sheet structure.[25,26] Our previous work found that the reconstructed defects caused the graphene sheets to exhibit remarkable wrinkling by distorting and deforming the defect lattice; compared to pristine graphene sheets, reconstructed defect sheets exhibit lower adhesion energy during the crumpling process resulting in hollow spherical crumpled structures, and the crumpled systems have larger bulk modulus and stronger stress heterogeneity levels due to sharper and stiffer crumples.[27] These MD simulation-based studies provide insight into the effects of damage and defects on sheet crumpling behaviors at the nanoscale.

In this work we build on this background by creating a set of experiments designed to explore the interplay between the materials and topography of a sheet in the crumpling process. Specifically, we introduce a set of cuts into the sheet aimed at disturbing any long-range features which may be important to the crumpling process, rather than removing area from the sheet. We work experimentally with both elastic and plastic materials, while at the same time using advanced coarse-grained molecular dynamic (CG-MD) simulations to explore observed effects. We note that such topological changes to the sheet have a very minor effect on the overall compressive strength. Remarkably, the cuts do strongly affect the location of high curvature features in the crumple. The two observations indicate that the overall crumple structure is not of primary importance to the compressive behavior.

2 Experimental

2.1 Materials

Polydimethylsiloxane (PDMS) is an easily crosslinked polymer with useful features such as hydrophobicity, optical transparency, biocompatibility, adhesion, flexibility, contamination resistance, durability and also a relatively low price. PDMS is often used as a protective layer for electrical insulation, anticorrosion, and antifouling coatings.[28] It is widely used in fabricating microfluidic devices,[29–32] microelectromechanical systems (MEMS),[33] as well as soft lithography stamps and molds.[34] In this work, we use the Dow-Corning Sylgard 184 system, which we cure at 80 degrees Celsius in a vacuum oven after mixing in a 10 to 1 ratio by weight of prepolymer to crosslinker. We regularly measure the modulus to be 1.69 MPa, which is in line with many other measurements in the literature.[35–37]

Polycarbonate (PC) is a thermoplastic material which has properties such as optical transparency, low weight, high modulus, and relatively high yield strength. PC can be used in optoelectronic devices as a replacement for inorganic glass substrates in flexible electronic devices.[38] The glass transition temperature, T_g of the PC is 145 °C.[35] Here, we use polycarbonate in chloroform solution to create thin sheets *via* spin coating, dip coating or drop casting. Additionally, we use some larger polycarbonate sheets purchased and used as received from McMaster-Carr. Cast sheets are cured above the PC T_g at approximately 200 °C. For both lab created and store bought PC we find Youngs modulus to be 2.0–2.6 GPa.[35,39–44]

Finally, we also use Quill.com multipurpose printer paper as an alternative high modulus, plastic material. We do so because even though the material is poorly controlled by us, is humidity dependent and is ultimately a tangle of fibers rather than a true continuum sheet, it can be made much more quickly and can increase the statistical power of our measurements. In our case, paper can be cut with a Cricut cutter in a manner of minutes, whereas PDMS and PC may take a day or more to properly cast a sheet. We find the paper to have a tensile modulus of 2×10^7 Pa and a thickness of 0.095 mm.

2.2 Sample preparation

2.2.1 PDMS preparation. PDMS solution is created by adding the Dow Corning Sylgard 184 pre-polymer base to the crosslinking curing agent in a 10 : 1 weight ratio. The mixture is then mixed thoroughly for about 10 minutes using a glass stirring rod. Degassing takes place inside a vacuum oven where the pressure is decreased and increased several times at room temperature. This removes air bubbles trapped inside the solution. After degassing, the solution is ready to be either spin coated or drop cast. Glass slide coated with a thin polyacrylic acid release layer was used as substrates when casting PDMS sheets. Samples are then placed inside the vacuum oven and annealed for 1 hour and 30 minutes at the curing temperature of 85 °C.

2.2.2 PC preparation. PC solution was created by adding polycarbonate polymer to the solvent Methylene Chloride in a 1% ratio using an electronic scale. The solution was kept at room temperature for two to three days to ensure the polymer is completely dissolved in the solvent. Freshly cleaved mica sheets are used as substrates for creating PC sheets. Mica is placed on a clean glass slide and held with the help of a water droplet in order to increase rigidity for spin-coating or drop-casting. Thinner PC sheets will be made by using the spin coating method. The glass/mica slide will be placed inside the spin-coater and the methylene chloride and PC solution is added using a glass pipet. The substrate is then annealed at 180 degrees Celsius for several hours.

Additionally, store bought sheets of polycarbonate were used in the large-scale setup. Here, sheets cut from a roll of 128 μm thick PC and were otherwise used as received from McMaster Carr inc. Sheets did not have any residual curvature due to shipping and storage and were found to have a modulus in the

Open Access Article. Published on 19 January 2023. Downloaded on 7/17/2025 10:22:53 PM.
This article is licensed under a Creative Commons Attribution-NonCommercial 3.0 Unported Licence.

same range as that measured with the thinner in-lab cast sheets.

2.2.3 Spin coating. As the first step, a clean substrate that will be covered with a polymer is placed in the middle of the spin coater. Next, the substrate is carefully secured to the spin coater by supplying vacuum to the chuck. Some amount of solution is then released on the middle of the substrate using a pipet. The spin coater is turned on and accelerates to the desired speed (acceleration and angular speed can be adjusted to create different sheet thicknesses). After allowing the coater to operate for a desired time, a very thin layer of polymer is left on top of the substrate.

2.2.4 Drop casting. In the drop-casting method, polymer solution was added to a container dropwise until it uniformly spread over the bottom of the whole container and achieved the desired thickness. If the solution is not uniform, holding the container at some angle will allow the gravity to spread the solution uniformly throughout the container. The solution will be placed on a flat, level surface to achieve further uniform spreading.

2.2.5 Sheet dimensions. The thickness of the sheets are measured using a confocal microscope before crumpling the sheet. The radius of the crumple is typically measured by taking a smartphone picture with a reference scale and using imageJ image processing software. Width and height measurements are also taken by image processing a smartphone image before crumpling. Thicknesses were measured with a confocal microscope, or *via* smartphone and image analysis software.

2.2.6 Minimizing adhesion. The elastic polymer PDMS involves adhesion that may confound results. Therefore, we remove adhesion by adding a monolayer of corn starch particles to both sides of sheet. There is no appreciable adhesion that needs to be removed from the PC sheets at the thicknesses used in this work.

2.2.7 Kirigami patterns. PDMS sheets were cut by hand with a scalpel blade. In particular, we add a button-hole like cut in the middle of the non-Sticky PDMS square as shown in Fig. 4a. This ensures the overall dimensions of the sheet are maintained. Typically, a sheet would first be tested in its native (sticky) state, then carefully uncrumpled. It was then treated to remove adhesion and recrumpled and tested. The process was then repeated while adding one, three or seven cuts before recrumpling. In this way, the exact same sheet can be examined in several different topological states.

On the other hand, plastic sheets were not reused. The paper and polycarbonate sheets could be cut with a cricut cutter controlled by a computer. This allowed more complex patterns to be cut (see Fig. 4a) in addition to the long straight 'button hole' cuts. Some sheets were cut by hand to mimic the slight imperfections that would be present in the PDMS sheets. sheets were often photographed after opening.

2.3 Mechanical testing

2.3.1 Confocal microscope. A typical experiment in the confocal setup is shown in Fig. 2. The sticky crumple shown in this figure is made out of PDMS with a 10 : 1 crosslink ratio

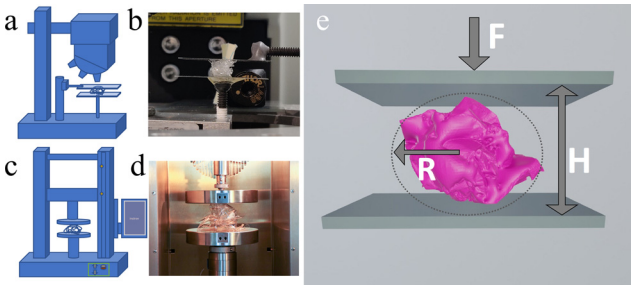

Fig. 2 Experimental setup. (a) Schematic diagram and (b) photograph of a crumple sample placed under confocal microscope. (c) Schematic diagram (d) photograph of a crumple sample placed under Instron. (e) Schematic diagram of a crumple showing applied force F, plate separation H and the radius R.

and the thickness of the crumple is between 50 μm to 100 μm. This simple experiment is designed to find the force response of the polymer crumple when compressed between two plates, while allowing detailed observation *via* microscopy. In this apparatus the bottom glass plate is connected to the force sensor (transducer technologies) and the top glass plate is connected to a sensitive motor (Physik Instrumente N-381.3a). A square shaped sheet is crumpled by hand. There is no exact procedure for crumpling to ensure it is always a random collection of folds and bends. After the crumple arrives at an approximately spherical shape, it is loaded between two parallel plates made of glass. Then the glass plates are moved close to each other until an arbitrary critical force value is reached, while force and distance data is recorded by a transducer and digital camera respectively.

2.3.2 Instron. A typical experiment in the Instron universal test machine setup is shown in Fig. 2. Here the larger industrially made PC sheet is crumpled and placed between the stainless-steel compression plates of an Instron 3400 universal testing system. The plates were set to move at a velocity of 5 mm min^{-1} for all experiments. Once again, force-displacement data is captured by the instrument, and imaging is conducted with a cell-phone camera.

3 Overview of coarse-grained modeling

This paper employs CG-MD simulations to investigate the compressive strength of crumpled graphene nanosheets having different cut patterns and to provide an in-depth analysis of the internal structure of the crumpled kirigami sheets. In brief, we obtained square graphene sheet models with 50 nm edge lengths having different cut patterns by removing specific combinations of CG beads on the previously developed graphene CG models.[45] That is, for the straight cut pattern (*i.e.*, 7 and 15 straight cuts), all CG beads in a straight line are deleted; for the Y cut pattern (*i.e.*, small and big Y cuts), multiple CG beads that form the Y-shape are deleted. After obtaining stable models that are in equilibrium, we apply a confining sphere that completely encompasses the model to simulate the

 This journal is © The Royal Society of Chemistry 2023

Open Access Article. Published on 19 January 2023. Downloaded on 7/17/2025 10:22:53 PM.
This article is licensed under a Creative Commons Attribution-NonCommercial 3.0 Unported Licence.

crumpling behavior of graphene sheets in experiments based on the aerosol evaporation method.[46] By decreasing the radius of the confining sphere at a speed of 50 m s^{-1} (consistent with previous studies),[27,47,48] the sheet model is compacted into a crumpled system accordingly and the crumpled system with a cylindrical shape is subsequently obtained by replacing the confining sphere with a confining cylinder. Note that the radius, height, and density of the crumpled cylindrical graphene before the uniaxial compression simulation are 7.1 nm, 14.9 nm, and 0.809 g cm^{-3}, respectively.

Next, uniaxial compression and unloading are performed by two rigid flat plates with the same material properties as the crumpled graphene sheet. Specifically, both uniaxial compression and unloading in our work are carried out at rates ranging from 40 m s^{-1} to 100 m s^{-1}, and the height and density of the cylindrical crumpled sheet in the final compressed state are 5 nm and 2.428 g cm^{-3}, respectively. Moreover, 130 independent simulations of crumpling, uniaxial compression, and unloading were performed for each cut pattern of the crumpled system. A detailed description of the CG graphene model, cut patterns, crumpling and uniaxial compression simulations can be found in ESI.† In our study, all CG-MD simulations are performed with the open-source package Large-scale Atomic/Molecular Massively Parallel Simulator (LAMMPS).[49]

4 Results and discussion

4.1 PDMS

Fig. 3 shows typical force displacements curves collected during an experiment. In this case a 32 mm by 40 mm sheet of thickness 75 μm was crumpled and tested first in the sticky,

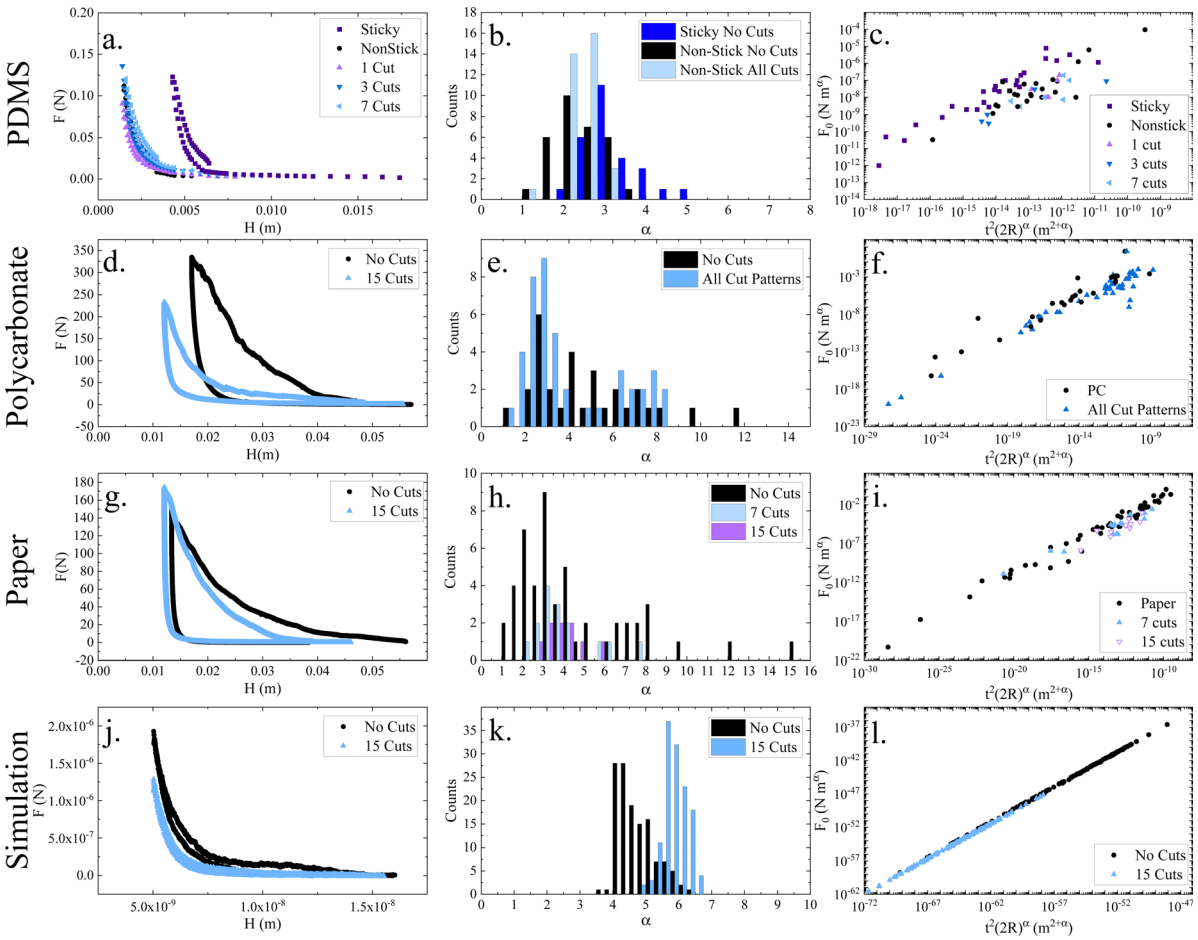

Fig. 3 Experimental and simulated results. PDMS experiments. (a) Representative force displacement curves of crumpled PDMS sheets in several states (sticky, non-sticky, cut non-sticky). (b) Histograms of the power law exponent recorded for each class of experiment (again sticky, non-sticky, cut non-sticky). (c) Power law amplitude as a function of $t^2(2R)^\alpha$. On this scaling plot, data falls along a linear curve, the height of which represents an effective modulus of the sheet. PC experiments. (d) Representative force displacement curves for crumpled PC sheets with no cuts or 15 straight cuts. (e) Histograms of the power law exponent recorded for cut and uncut PC sheets. (f) Power law amplitude as a function of $t^2(2R)^\alpha$. Cut data might be slightly lower, indicating a reduced effective modulus. Paper experiments. (g) Representative force displacement curves for crumpled paper sheets with no cuts or 15 straight cuts added. (h) Histograms of the power law exponent recorded for cut and uncut paper sheets. (i) Power law amplitude as a function of $t^2(2R)^\alpha$. Cut data is slightly lower, indicating a reduced effective modulus. CG-MD graphene simulations (j) representative force displacement curves for crumpled graphene sheets with no cuts or 15 straight cuts added. (k) Histograms of the power law exponent recorded for cut and uncut crumpled graphene sheets. (l) Power law amplitude as a function of $t^2(2R)^\alpha$. Cut data is slightly lower, indicating a reduced effective modulus.

Open Access Article. Published on 19 January 2023. Downloaded on 7/17/2025 10:22:53 PM.
This article is licensed under a Creative Commons Attribution-NonCommercial 3.0 Unported Licence.

as produced state, shown by the black solid circle symbols. The curve is well fit by a power law, as is expected. The sheet was then carefully uncrumpled and treated to remove surface adhesion. The sheet was then recrumpled and retested producing the curve shown by the gray solid square symbols in Fig. 3a. Notably, the adhesion free sheet is much more compressible than the sticky sheet, a phenomenon discussed previously in ref. 23. The uncrumpling/recrumpling process was then repeated with straight cuts added on each subsequent uncrumpling. The data for crumples with 1, 3, and 7 cuts are shown in Fig. 3a. We note some small variation in the force curves; however, the variation is not correlated with the number of cuts. The observed differences are typical of repeated crumple measurements even when no topological changes are made to a sheet. Each test involves completely opening and recrumpling the PDMS sheet, so each force curve probes a different crumpled network. In short, the force displacements curves show no sensitivity to the topological changes of the sheet due to the cuts.

To look more carefully at the data, each force–displacement curve was fit with a power law $F = F_0H^{\alpha}$. Fig. 3b shows a histogram of the various α values recorded from the fits. The distribution of the sticky sheet exponents may fall on slightly higher values than does the non-sticky sheets, however, within the statistics we have collected no claim can be made that the distributions are significantly different.

Next, in Fig. 3c we plot the fit values for the power law amplitude (F_0) against the expected scaling predicted by eqn (1), leaving the modulus as a fit parameter. The plot shows the sticky sheet data to lie along a straight line (on a log–log axis) and to have a higher effective modulus (as it is higher along the y axis), than the low adhesion tests. The low adhesion sheets and the cut low adhesion sheets also lie along a straight line, but once again no difference can be reliably observed between the cut and uncut sheets. In summary, the PDMS sheets do not show any statistically significant differences when cuts are added to change the sheet topology.

4.2 PC

It is possible that PDMS sheets do not show differences with topological changes because they are elastic and have a relatively low modulus. Polycarbonate, on the other hand, has a much higher modulus and will plastically yield in regions of high stress. It can therefore serve as a good alternative material system to broaden this investigation. Hence, experiments were conducted in a similar manner as was described above with PDMS sheets. Once again, power laws were fit to force–displacement data taken with uncut and cut PC sheets. Note that unlike the PDMS experiments, each PC sheet is used only once due to the memory created by plasticity.

Fig. 3d shows force–displacement curves recorded for a typical uncut and a typical cut PC crumpled sheet. Curves show some small but near instant changes in force, which correspond to stick-slip or buckling events within the crumple. These are not noted in the experiments with very thin sheets, possibly due to their increased adhesion. Regardless, the overall indentation curves are still well fit with a power law, so again an exponent and amplitude could be measured. We also note the much greater hysteresis in the PC sheets, due to the plastic loss occurring during compression. Again, there is very little quantifiable difference between the cut sheets and the uncut sheets.

Histograms of the power law exponents for both cut and uncut polycarbonate sheets are shown in Fig. 3e. Both distributions appear to be log-normal (rather than Gaussian as the PDMS sheets), and there again appears to be little difference between the cut and uncut sheets.

Fig. 3f shows the amplitude of the power law fit on the same scaling plot as discussed in Fig. 3c. The data for all uncut sheets, straight cut sheets and Y cut sheets appears to fall along straight lines, reinforcing the broad applicability of eqn (1). Both sets of cut sheets (straight and Y) appear slightly lower on the plot, indicating a possible decrease in effective modulus, but the observation is not outside the scatter in the data and is once again inconclusive.

4.3 Paper

In order to more easily increase statistics and add an additional material to this study, experiments were conducted on paper sheets. Sheet size, cut number, and cut pattern were varied. Room relative humidity was typically around 60% during the experiments. Representative results are shown in Fig. 3 taken from experiments following the same protocol as with the other two materials.

Force curves for both pristine sheets and cut sheets show very similar behavior and are well fit by power law curves. Histograms of the power law exponents show a log-normal distribution for both cut and uncut sheets and a slight increase for the peak of the distribution with increasing number of cuts in the sheets (Fig. 3b). Power law amplitudes also show a slight difference, with the cut sheets being slightly lower in effective modulus than uncut sheets. Average modulus for all three materials calculated by fitting eqn (1) above are reported in Table 1 below for clarity.

4.4 Molecular dynamics compression simulation of coarse-grained crumpled graphene

We conducted CG-MD simulations of many different cut patterns (see Fig. S1 in ESI†), but to follow experiments, we only compare and analyze the details of uncut and 15 straight cuts crumpled graphene sheets to explore the effect of topological changes in the sheets on their mechanical properties at the nanoscale. As shown in Fig. 3j, the MD simulation validates that the relationship between the compressive force and the plate separation can be well described by eqn (1) for the crumpled graphene model with two different topologies (*i.e.*, no cuts and 15 straight cuts). In addition, the force–displacement cycle of the uncut sheet shows a slightly larger compliance and hysteresis than that of the 15 straight cuts sheet. We believe that this is because the cut sheet is more mobile during the crumpling process. The cut model forms more short-range

 This journal is © The Royal Society of Chemistry 2023

Open Access Article. Published on 19 January 2023. Downloaded on 7/17/2025 10:22:53 PM.
This article is licensed under a Creative Commons Attribution-NonCommercial 3.0 Unported Licence.

Table 1 Average plane strain modulus measured *via* crumpling

	Modulus (Pa)	
Material	Uncut sheets	Cut sheets
PDMS	$1.8 \times 10^5 \pm 3 \times 10^5$	$1.1 \times 10^5 \pm 9 \times 10^4$
PC	$5.7 \times 10^8 \pm 9 \times 10^8$	$6.4 \times 10^7 \pm 9 \times 10^7$
Paper	$2.3 \times 10^9 \pm 3 \times 10^9$	$6.7 \times 10^8 \pm 1 \times 10^9$
Simulations	$1.4 \times 10^{11} \pm 6 \times 10^{10}$	$5.2 \times 10^{10} \pm 3 \times 10^{10}$

laminated bends during crumpling (see Fig. S2a in ESI†), requiring less force during compression.

The histogram of power law exponents in Fig. 3k shows that the power law exponents of the 15 straight cuts model increase with respect to the no cuts model and exhibit narrow, possibly log normal distributions. Further, the relationship between F_0 and $t^2(2R)$ indicates that the MD simulation data obey a linear relationship and the fitted line of the 15 straight cuts model lies slightly below the no cuts model, implying that the 15 straight cuts crumpled model has a slightly smaller effective modulus (Fig. 3l). Notably, the effects of cuts on the compressive properties of the sheet observed in the simulations are in general consistent with the phenomena observed in the experiments (especially for crumpled PC and paper), suggesting that the influence of cuts on the mechanical properties of the sheet is valid at both the nano- and macro-scale and is again fairly small.

To better understand the effect of topological changes on the internal structure of the crumpled sheet, Fig. 4 proceeds to analyze the local curvature, von Mises stress, and typical cross-section patterns of the crumpled graphene sheet after uniaxial compression in simulation. The local von Mises stress (σ_v) is given by $\sigma_v = \sqrt{(3\sigma_{ij}\sigma_{ij} - \sigma_{kk}^2)/2}$, where σ_{ij} (i,j = 1,2,3) are the components of the Cauchy stress tensor. Note that the von Mises stress considered in this work is normalized with respect to volume of the model and that it is a theoretical value that can be utilized as a yielding criterion (*i.e.*, σ_v is not a real stress); the local curvatures and stresses are mapped to a 2D planar model for better visualization. Fig. 4a and b show the local curvature and stress distribution of the crumpled graphene sheets with different cut patterns (*i.e.*, no cuts, small and big Y cuts, and 7 and 15 straight cuts) after uniaxial compression, respectively. It can be observed that the high curvature regions of all models correspond closely to their high stress regions. High curvature and stress regions of models with cuts exhibit short-range and isolated patterns compared to the long-range and interconnected high curvature and stress regions presented by the no cuts model. This is attributed to the introduction of cuts (especially straight cuts) that make the sheet tend to form laminated bends during the crumpling process, while forming fewer d-cones and ridges, and the cut pattern breaks the internal structure of the crumpled system. Fig. 4c and d present the probability distributions of the local curvatures and stresses of the crumpled model after uniaxial compression, which are observed to be skewed log normal and normal distributions, respectively. In detail, the introduction of the cut causes the peak of the curvature probability distribution to decrease, while the peak of the stress probability distribution increases and shifts to a lower stress, indicating that the cut makes the crumpled system less mechanically heterogeneous, as well as reducing the effective modulus of the system (Fig. 4e). Furthermore, the distribution of curvature *versus* stress (Fig. 4f) can be reconfirmed that the stress and curvature of the no cuts model and the cuts model remain highly correlated, *i.e.*, small curvature corresponds to small stress and large curvature corresponds to large stress, only with relatively small curvature and stress of the cuts model.

To provide a better illustration of the influence of cuts on the internal structure of the crumpled system at the nanoscale, Fig. 4g shows the cross-section patterns of the no cuts model and the 15 straight cuts model before and after uniaxial compression, repectively, which are obtained by cutting the crumpled system with a cutting plane perpendicular to the compressing plates. It can be found that the no cuts model displays an ordered long-range laminated cross-section pattern both before and after uniaxial compression, while the 15 straight cuts model shows more ordered and short-range laminated cross-sections (highlighted in blue for examples) before and after uniaxial compression. This again indicates that the cuts of the sheet allow the internal structure of the crumpled system to be cut off, which further affects the mechanical properties of the system. In general, the effective modulus decreases sequentially in the order of no cuts, small Y cuts, big Y cuts, 7 straight cuts, and 15 straight cuts (Fig. 4e), *i.e.*, from $1.36 \times 10^{11} \pm 0.58 \times 10^{11}$ Pa in the no cuts model to $2.53 \times 10^{10} \pm 0.77 \times 10^{10}$ Pa in the 15 straight cuts model. Although the drop in effective modulus is close to an order of magnitude, it is a relatively small reduction and not as significant as one might expect. As with the experimental findings, the topological change produces a relatively significant effect on the internal structure of the crumpled sheet at the nanoscale, whereas the effect on its compressive strength is relatively small, implying that the ridges and other long-range structures in the crumpled system have a small effect on the overall compressive strength of the system.

4.5 Line detection

In the experimental system, it is difficult to quantify structural features of the crumpled sheets without complex 3D imaging techniques.[10,50] However, both the PC and the Paper sheets deform plastically during crumpling which means that there is a visible memory of high curvature regions of the internal network of the crumple after a sheet has been carefully uncrumpled. As is common in the literature, we examine this structure *via* scanning sheets and processing the images (see Fig. 5).[11–13]

Here we examine paper crumples by first carefully uncrumpling a sheet after an experiment and then using a black marker to emphasize all the long-range structures that were visible (*i.e.* folds in the crumple). Basic line detection of a photo of the flattened crumpled sheet was completed with a code written in python. The line detection method was imperfect, so each data set was additionally screened for any flaws. Any flaws were

Open Access Article. Published on 19 January 2023. Downloaded on 7/17/2025 10:22:53 PM.
This article is licensed under a Creative Commons Attribution-NonCommercial 3.0 Unported Licence.

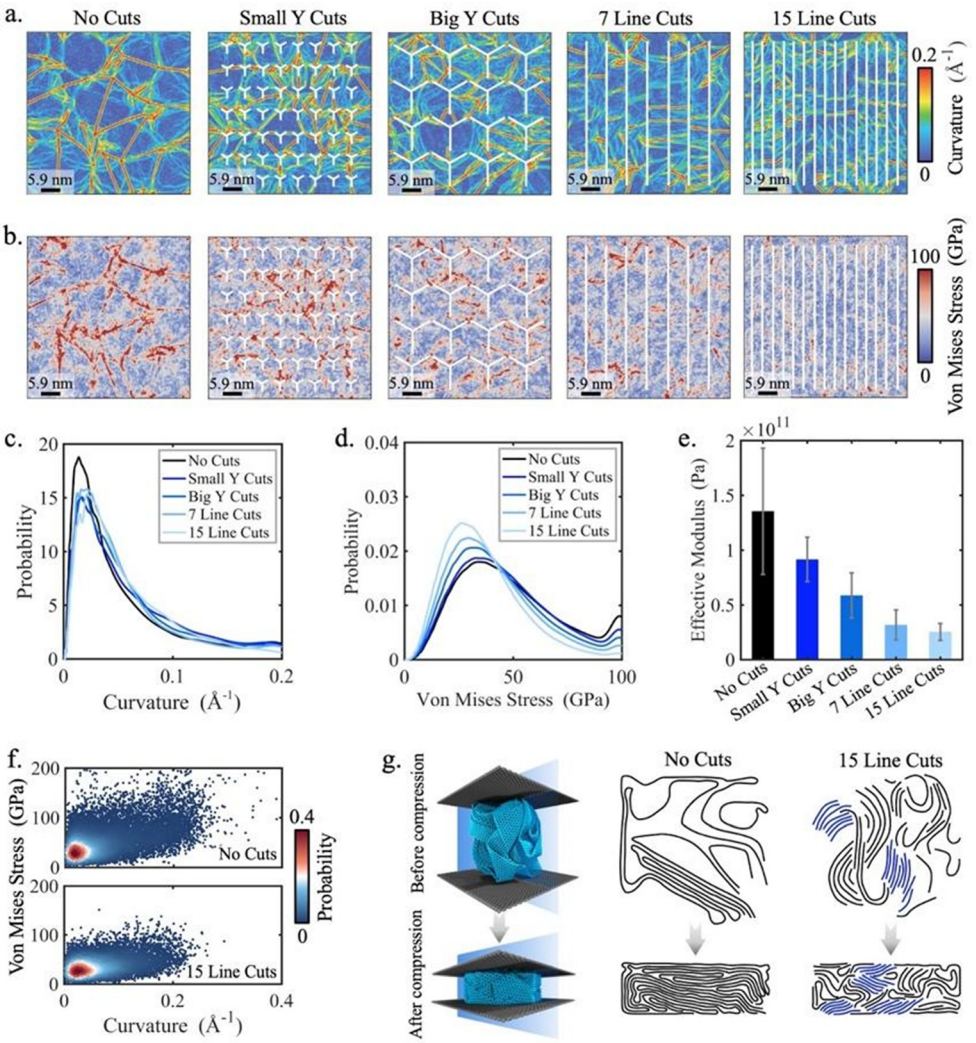

Fig. 4 Internal structure analyses of crumpled graphene. Local (a) curvature and (b) von Mises stress distribution maps for crumpled graphene sheets with different cut patterns after uniaxial compression simulation (before unloading). The probability distributions of local (c) curvature and (d) von Mises stress. (e) Effective modulus of crumpled graphene sheets with different cut patterns. (f) Distributions of curvature *versus* von Mises stress crumpled graphene sheets having no cuts and 15 straight cuts, respectively. (g) Schematics for analyzing the cross-section patterns of the crumpled model before and after the uniaxial compression simulation, and the corresponding cross-section patterns of the no cuts and 15 straight cuts models. The ordered short-range laminate structure is highlighted in blue in the 15 straight cuts model.

subsequently corrected by hand using ImageJ software. Ultimately a table of line segments was constructed, where each line represented a crease in the uncrumpled paper sheet.

A similar process could be used to analyze the simulated sheets. In this case regions of high curvature were marked by software during the peak of compression in an experiment. The sheet could the be digitally unfolded into a flat state, and lines could be fit to the high curvature regions by adjusting a curvature threshold. Again, a table of line segments could be prepared and analysed.

The tables of lines could then be studied in several ways. We considered the angle made by a typical fold and the horizontal (Fig. 5). Uncut paper sheets have a uniform distribution of angles, which is not surprising; the sheet is homogeneous and there is no strong case for any symmetry breaking. The same result also occurred with the uncut simulated graphene sheets. However, the angular distribution from both cut paper and simulated graphene showed a bias towards folds having an angle of zero. In other words, the high curvature regions preferentially align perpendicularly to the cut edges. The transition angle differed between experiment and simulation, which we believe is related to the plasticity of paper which is not present in the simulations. This is because the elastic simulated sheets are more free to rearrange regions of high curvature as confinement is increased, whereas plasticity will lock in a feature above a threshold curvature in the paper sheets. The mobility in the simulation allows features to further reduce their energy by decreasing their total length.

Analysis could also consider the average length of the lines. We expect this part of the analysis to be less quantitative, and thus defer it to the ESI.† There is some arbitrariness to assigning the beginning and end points for the straight-line segments

 This journal is © The Royal Society of Chemistry 2023

Open Access Article. Published on 19 January 2023. Downloaded on 7/17/2025 10:22:53 PM.
This article is licensed under a Creative Commons Attribution-NonCommercial 3.0 Unported Licence.

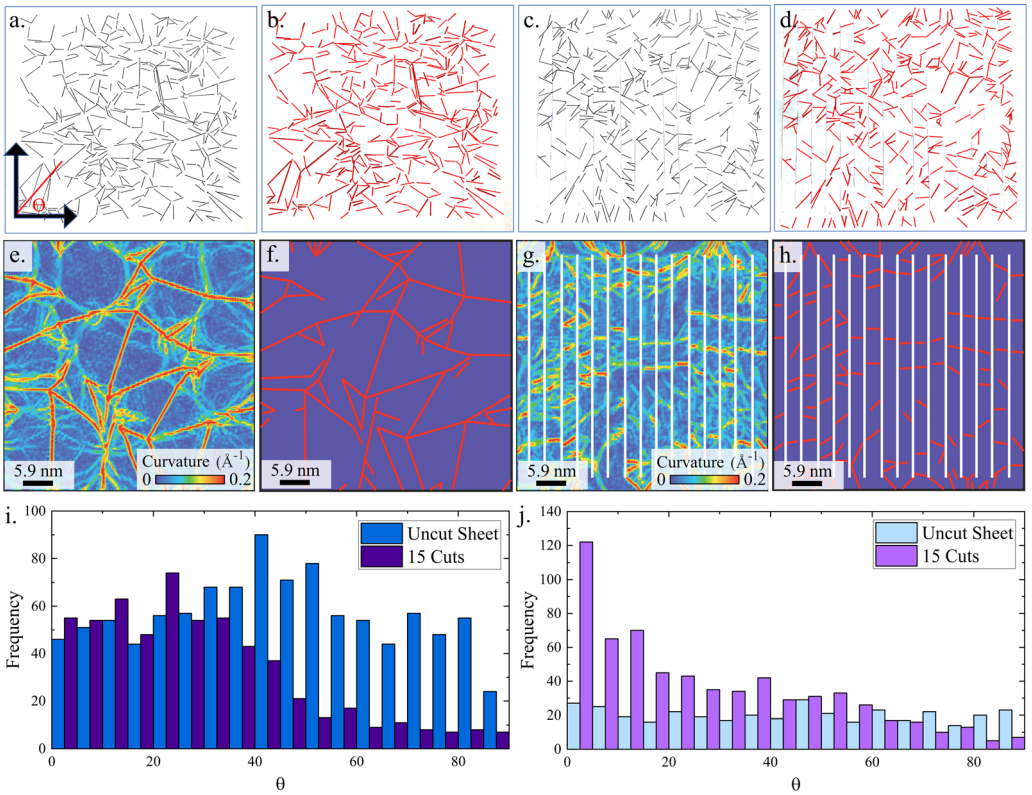

Fig. 5 Curvature detection in experiments and simulations. (a) Photo of a uncut and uncrumpled paper crumple (b) line detected uncut paper crumple (c) photo of 15 cuts uncrumpled paper crumple. (d) Line detected 15 cuts paper crumple. Note that at the contrast required for crease detection, the thin cuts are difficult to see in the images. (e) Local curvature distribution and (f) detected high curvature regions of uncut crumpled graphene simulations. (g) Local curvature distribution and (h) detected high curvature regions of 15 cuts crumpled graphene simulation. (i) Orientation of the ridges in paper crumple. (j) Orientation of the ridges in simulated crumpled graphene. Here, both uncut and cut crumpled sheets are obtained from five independent simulations.

in both simulations and experiments (we do not attempt to force lines to begin or end on other lines or edges in order to create polygonal facets). This is in part due to the arbitrary threshold for observation (a line occurs only where bending stress is above the yield stress, or some curvature for simulations). In short, we find a reduction in the number of long segments in cut sheets, as was our basic hypothesis. A second interesting observation of this analysis is that crumpled sheets and cut crumpled sheets of similar density tended to have similar overall total line lengths. This is in agreement with the observations of Gottesman *et al.*,[12] in that the total line length correlates with the compression resistance of the crumple.

5 Conclusions

In this work we conducted simple compression experiments and simulations on crumpled sheets with and without kirigami-like cut patterns. Experiments examined three different materials (PDMS, PC and Paper). No significant differences between cut and uncut sheets of the elastomeric PDMS samples could be detected in experiments. On the other hand, plastic materials (PC and Paper) show small changes in effective modulus when cut. CG-MD simulations were conducted on a model graphene sheet and results showed that cut graphene behaved similarly to the plastic experimental materials – small changes in the stiffness of the crumpled sheets were noted.

The CG-MD results also allow a detailed look at the internal structure and stress state of the crumples, where few significant changes were noted in the crumpled cut sheets compared to the uncut sheets. Of note, the location and orientation of the highly curved regions of the sheet (creases) were significantly altered by the cut patterns. Both simulated data and experimental data were analyzed by assigning a line segment to each visible crease (or high curvature region). Line segment ensembles showed a distinct perpendicular orientation to cut edges, which was more pronounced in higher density crumples. Because the overall changes in compression behavior were small, while the structural changes in the highly curved parts of a sheet was significant, we conclude that the orientation and patterns formed by the internal network of creases during crumpling are not significant to the macroscopic compressive behavior.

The similarity between cut and uncut crumpled sheets means that long range structures like the ridges shown in Fig. 4c. cannot play a significant role in the compression modulus of a crumpled sheet. Similarly, because the total length of the folds remained similar between cut and uncut sheets, while the orientation and length distributions differed,

Open Access Article. Published on 19 January 2023. Downloaded on 7/17/2025 10:22:53 PM.
This article is licensed under a Creative Commons Attribution-NonCommercial 3.0 Unported Licence.

the idea of a fold as a long-range structure cannot be correct. This fits well with the conceptual model of a fold simply being a loci of point-like defects – the number of defects matters, not their orientation.

Author contributions

W. J. conceptualized the study, lead the experimental data collection, analysed data and wrote the original draft. Y. L. conceptualized, acquired, and analysed computational data, contributed to the writing the manuscript, reviewed, and edited the manuscript. Z. L. contributed to the computational data acquisition. W. X. conceptualized the study, led the computational effort, supervised Y. L. and Z. L., acquired funding, and reviewed and edited the manuscript. A. B. C. conceptualized the study, led the experimental team, supervised W. J., contributed to data acquisition and analysis, acquired funding, and reviewed and edited the manuscript.

Conflicts of interest

There are no conflicts to declare.

Acknowledgements

The authors acknowledge the support from the Army Research Office (award no. W911NF2010208). The simulations of this work used resources of the Center for Computationally Assisted Science and Technology (CCAST) at North Dakota State University, which were made possible in part by NSF MRI award no. 2019077.

References

1 P. K. Purohit, J. Kondev and R. Phillips, *Proc. Natl. Acad. Sci. U. S. A.*, 2003, **100**, 3173–3178.
2 E. Katzav, M. Adda-Bedia and A. Boudaoud, *Proc. Natl. Acad. Sci. U. S. A.*, 2006, **103**, 18900–18904.
3 H. Kobayashi, B. Kresling and J. F. V. Vincent, *Proc. R. Soc. London, Ser. B*, 1998, 147–154.
4 B. Mota and S. Herculano-Houzel, *Science*, 2015, **349**, 74–77.
5 J. Plescia and M. Golombek, *Geol. Soc. Am. Bull.*, 1986, **97**, 1289–1299.
6 M. F. Ashby, *Philos. Trans. R. Soc., A*, 2006, **364**, 15–30.
7 N. P. D. Luca, O. M. Reyes and P. M. Jacques, *Inflatable, cushioning, bubble wrap product having multiple, interconnected, bubble structures*, *US Pat.*, US6410119B1, 2000, **https://patents.google.com/patent/US6410119B1/en**.
8 K. Matan, R. B. Williams, T. A. Witten and S. R. Nagel, *Phys. Rev. Lett.*, 2002, **88**, 076101.
9 S. Deboeuf, E. Katzav, A. Boudaoud, D. Bonn and M. Adda-Bedia, *Phys. Rev. Lett.*, 2013, **110**, 104301.
10 A. B. Croll, T. Twohig and T. Elder, *Nat. Commun.*, 2019, **10**, 1–8.
11 D. L. Blair and A. Kudrolli, *Phys. Rev. Lett.*, 2005, **94**, 166107.
12 O. Gottesman, J. Andrejevic, C. H. Rycroft and S. M. Rubinstein, *Commun. Phys.*, 2018, **1**, 70.
13 J. Andrejevic, L. M. Lee, S. M. Rubinstein and C. H. Rycroft, *Nat. Commun.*, 2021, **12**, 1470.
14 T. Mora and A. Boudaoud, *Europhys. Lett.*, 2002, **59**, 41–47.
15 M. K. Blees, A. W. Barnard, P. A. Rose, S. P. Roberts, K. L. McGill, P. Y. Huang, A. R. Ruyack, J. W. Kevek, B. Kobrin and D. A. Muller, *et al.*, *Nature*, 2015, **524**, 204–207.
16 P. Wang-Iverson, R. J. Lang and Y. Mark, *Origami 5: Fifth International Meeting of Origami Science, Mathematics, and Education*, CRC Press, 2011.
17 Y. Liu, J. Genzer and M. D. Dickey, *Prog. Polym. Sci.*, 2016, **52**, 79–106.
18 Y. Liu, B. Shaw, M. D. Dickey and J. Genzer, *Sci. Adv.*, 2017, **3**, e1602417.
19 J. Tao, H. Khosravi, V. Deshpande and S. Li, *Adv. Sci.*, 2022, 2204733.
20 G. A. Vliegenthart and G. Gompper, *Nat. Mater.*, 2006, **5**, 216–221.
21 T. Tallinen, J. Åström and J. Timonen, *Nat. Mater.*, 2009, **8**, 25–29.
22 M. Habibi, M. Adda-Bedia and D. Bonn, *Soft Matter*, 2017, **13**, 4029–4034.
23 A. B. Croll, Y. Liao, Z. Li, W. M. Jayawardana, T. Elder and W. Xia, *Matter*, 2022, 1792–1805.
24 M. J. Mirzaali, M. Habibi, S. Janbaz, L. Vergani and A. A. Zadpoor, *Sci. Rep.*, 2017, **7**, 13028.
25 I. Giordanelli, M. Mendoza, J. S. Andrade Jr, M. Gomes and H. J. Herrmann, *Sci. Rep.*, 2016, **6**, 1–6.
26 S. W. Cranford and M. J. Buehler, *Phys. Rev. B: Condens. Matter Mater. Phys.*, 2011, **84**, 205451.
27 Y. Liao, Z. Li, W. Nie and W. Xia, *Forces Mech.*, 2022, **6**, 100057.
28 K. Efimenko, W. E. Wallace and J. Genzer, *J. Colloid Interface Sci.*, 2002, **254**, 306–315.
29 E. Sollier, C. Murray, P. Maoddi and D. Di Carlo, *Lab Chip*, 2011, **11**, 3752–3765.
30 J. C. McDonald and G. M. Whitesides, *Acc. Chem. Res.*, 2002, **35**, 491–499.
31 G. M. Whitesides, *Nature*, 2006, **442**, 368–373.
32 D. Armani, C. Liu and N. Aluru, Technical Digest. IEEE International MEMS 99 Conference. Twelfth IEEE International Conference on Micro Electro Mechanical Systems (Cat. No. 99CH36291), 1999, pp. 222-227.
33 F. Schneider, J. Draheim, R. Kamberger and U. Wallrabe, *Sens. Actuators, A*, 2009, **151**, 95–99.
34 Y. Xia and G. M. Whitesides, *Annu. Rev. Mater. Sci.*, 1998, **28**, 153–184.
35 T. Elder, D. Rozairo and A. B. Croll, *Macromolecules*, 2019, **52**, 690–699.
36 I. D. Johnston, D. K. McCluskey, C. K. L. Tan and M. C. Tracey, *J. Micromech. Microeng.*, 2014, **24**, 035017.
37 T. K. Kim, J. K. Kim and O. C. Jeong, *Microelectron. Eng.*, 2011, **88**, 1982–1985.
38 T. Hanada, T. Negishi, I. Shiroishi and T. Shiro, *Thin Solid Films*, 2010, **518**, 3089–3092.

 This journal is © The Royal Society of Chemistry 2023

Open Access Article. Published on 19 January 2023. Downloaded on 7/17/2025 10:22:53 PM.
This article is licensed under a Creative Commons Attribution-NonCommercial 3.0 Unported Licence.

39 C. Bauwens-Crowet, J. C. Bauwens and G. Homès, *J. Polym. Sci., Part A-2*, 1969, **7**, 735–742.
40 A. Flory and G. B. McKenna, *Mech. Time-Depend. Mater.*, 2010, **14**, 347–357.
41 J. M. Hutchinson, S. Smith, B. Horne and G. M. Gourlay, *Macromolecules*, 1999, **32**, 5046–5061.
42 J. M. Hutchinson, A. B. Tong and Z. Jiang, *Thermochim. Acta*, 1999, **335**, 27–42.
43 M. J. Mindel and N. Brown, *J. Mater. Sci.*, 1973, **8**, 863–870.
44 V. A. Soloukhin, J. C. M. Brokken-Zijp, O. L. J. van Asselen and G. de With, *Macromolecules*, 2003, **36**, 7585–7597.
45 L. Ruiz, W. Xia, Z. Meng and S. Keten, *Carbon*, 2015, **82**, 103–115.
46 X. Ma, M. R. Zachariah and C. D. Zangmeister, *Nano Lett.*, 2012, **12**, 486–489.
47 Y. Liao, Z. Li and W. Xia, *et al.*, *Carbon*, 2021, **174** 148–157.
48 Y. Liao, Z. Li, S. Ghazanfari, Fatima, A. B. Croll and W. Xia, *Langmuir*, 2021, **37**, 8627–8637.
49 S. Plimpton, *J. Comput. Phys.*, 1995, **117**, 1–19.
50 A. Cambou and N. Menon, *Proc. Natl. Acad. Sci. U. S. A.*, 2011, **108**, 14741–14745.